

# Structural properties and relative stability of (meta)stable ordered, partially ordered, and disordered Al-Li alloy phases

Aftab Alam<sup>1,\*</sup> and D. D. Johnson<sup>1,2,†</sup><sup>1</sup>Ames Laboratory, U.S. Department of Energy, Ames, IA, 50011-3020<sup>2</sup>Department of Materials Science & Engineering, Iowa State University, Ames, Iowa 50011

(Received 8 February 2012; published 11 April 2012)

We resolve issues that have plagued reliable prediction of relative phase stability for solid solutions and compounds. Due to its commercially important phase diagram, we showcase the Al-Li system because historically density-functional theory (DFT) results show large scatter and limited success in predicting the structural properties and stability of solid solutions relative to ordered compounds. Using recent advances in an optimal basis-set representation of the topology of electronic charge density (and, hence, atomic size), we present DFT results that agree reasonably well with all known experimental data for the structural properties and formation energies of ordered, off-stoichiometric partially ordered, and disordered alloys, opening the way for reliable study in complex alloys.

DOI: [10.1103/PhysRevB.85.144202](https://doi.org/10.1103/PhysRevB.85.144202)

PACS number(s): 71.15.-m, 71.23.-k, 61.66.Dk, 64.60.Cn

## I. INTRODUCTION

Predicting alloy composition-temperature ( $x$  vs  $T$ ) phase diagrams has important practical implications, and much progress has been made in the last decade via *ab initio* study of phase stability. Such predictions are a sensitive test as the relative stability of metallic alloys depend on small enthalpy differences. Notably, the order-disorder temperature of a superstructure is related to the difference between the formation enthalpy of the compound  $\text{Al}_m\text{Li}_n$  [ $x = n/(n+m)$ ] and mixing enthalpy<sup>1</sup> of disordered  $\text{Al}_{1-x}\text{Li}_x$  alloy at the same composition  $x$  (Ref. 2). Historically, density-functional theory (DFT) results were sensitive to basis sets and approximations,<sup>3</sup> especially comparing ordering and mixing enthalpies from different codes.<sup>4</sup> In particular, representations of charge densities are critical, especially for solid solutions, where former “bad” results were not due, as often proposed, to the approximation to the disordered state.<sup>5</sup> How the disordered phases is addressed remains an ongoing issue, such as the longstanding discrepancies between approximations to partially ordered (off-stoichiometric and thermal antisites<sup>6</sup>) and disordered phases, for example, the coherent-potential approximation<sup>3,6-8</sup> (CPA), special quasirandom structures<sup>3,9,10</sup> (SQSs), and cluster expansions<sup>3,11-13</sup> (CEs).

Al-Li alloys, with their unusual elastic and structural properties and commercial importance, have been the focus of many theoretical and experimental studies. With doping to initiate precipitate growth in grains or grain boundaries, they are suitable materials for aerospace and automobile applications, due to their low density, high elastic modulus, and high strength-to-weight ratio. Between the stable end points of Al-Al (fcc) and Al-Li (bcc), numerous structural phases exist or compete,<sup>14</sup> for example, the stable  $\beta$  AlLi (B32), rhombohedral  $\text{Al}_2\text{Li}_3$  (C33), monoclinic  $\text{Al}_4\text{Li}_9$  (B2/m), and metastable (off-stoichiometric)  $\delta'$ - $\text{Al}_3\text{Li}$  ( $\text{L1}_2$ ). The  $\beta$  AlLi, for example, is a promising candidate as an anodic material in high-energy density batteries;  $\delta'$ , which appears in the miscibility gap between Al and  $\beta$ , is used to precipitation harden commercial alloys.<sup>15-17</sup> Substituting Li for Al not only makes the alloy less dense but increases unexpectedly the elastic moduli,<sup>18</sup> even though the Young’s modulus of Li

(14 GPa) is seven times smaller than that of Al (91 GPa). Also, the valence density leads to a bulk modulus of Al (83 GPa) five times larger than that of Li (15 GPa), giving rise to a sensitivity to basis sets if density is not represented properly.<sup>5</sup>

Comparing reliably properties of all competing phases in alloys is critical, and Al-Li is a sensitive, sufficiently complex, and yet unresolved case. While there are some successes in describing the relative stability of the Al-Li ordered phases,<sup>19-21</sup> a reliable description for the disordered and partially ordered phases is lacking. For Al-Li disordered phases, the virtual crystal approximation (VCA),<sup>22</sup> CPA,<sup>23</sup> and CE methods<sup>11,12</sup> have been used to describe the  $x$ -dependent equilibrium volume and formation enthalpies, but quantitative prediction of the lattice constants and mixing enthalpy remains a problem.

Using an optimal site-centered basis for density and potentials,<sup>5</sup> we present *ab initio* DFT calculations that compare reliably the phase stability (formation enthalpies) of competing ordered, partially ordered, and disordered phases, and quantitatively reproduce (without adjustable parameters) the unusual alloying effects, including the lattice constants, that is,  $a$  vs  $x$ , ill-described in the past. We also estimate the impurity formation energies at  $x \simeq 0$  and 1 (i.e., the solution enthalpies) of the  $\text{Al}-\text{Al}_{1-x}\text{Li}_x$ , a sensitive quantity due to differing electronic nature of Al and Li. For general configurations, we describe more properly the topology of electronic charge density, and hence atomic size, charge, and alloying effects, especially in random alloys,<sup>2,5,24</sup> crucial in Al-Li for a reliable investigation of (meta)stable phases.<sup>5</sup> We also resolve longstanding disagreements between various estimates of disordered energetics, for example, CPA<sup>7,8</sup> and SQS.<sup>3</sup> To showcase the predictive accuracy, we compare and contrast our results to experimental data and those from linear augmented plane wave (LAPW),<sup>19</sup> augmented spherical wave (ASW),<sup>20</sup> linear muffin-tin orbital (LMTO) methods, and atomic sphere approximation (ASA).

## II. COMPUTATIONAL DETAILS

We use a Korringa-Kohn-Rostoker (KKR) CPA code<sup>25</sup> based on a weighted Voronoi polyhedra (VP)<sup>26</sup> basis defined

from saddle-point radii (SPR) in the charge density.<sup>5</sup> With this optimal basis set, a proper representation of the topology of charge density and hence atomic sizes yields energy differences insensitive to basis-set  $L$  truncation.<sup>2,5</sup>

We include  $s$ -,  $p$ -,  $d$ -, and  $f$ -symmetries in the KKR Green's functions spherical harmonic basis, which is truncated at  $L_{\max} = 3$ , where  $L \equiv (l, m)$ . Energy integration of Green's functions use a complex-energy Gauss-Chebyshev semicircular contour with 18 points. The Brillouin zone integrations use the Monkhorst and Pack<sup>27</sup> special  $k$ -point method using a  $20 \times 20 \times 20$  mesh. We use the von Barth-Hedin<sup>28</sup> local density approximation (LDA) as parameterized by Moruzzi, Janak, and Williams.<sup>29</sup> For random alloys, the screened CPA<sup>8</sup> is used to incorporate metallic screening from charge correlations in the local chemical environment. More details are given elsewhere.<sup>2,5,24</sup>

The lattice constants of the elemental Al and Li, Al Al-Li, and B32 phases were calculated for comparison to experiment, as were the metastable phases, such as L1<sub>0</sub>. The relaxation effects on some of the less symmetric structures are mostly small, as noted in text.

The potential zero, that is, *muffin-tin zero*  $v_0$ , can dramatically affect stability prediction for spherical potentials. We use a variational definition ( $X$  stands for VP or ASA),

$$v_0^X = \frac{\sum_s \int_{\text{MT}}^X d\mathbf{r} \rho_s^{\text{FP}}(\mathbf{r}) V_s^{\text{FP}}(\mathbf{r})}{\sum_s \int_{\text{MT}}^X d\mathbf{r} \rho_s^{\text{FP}}(\mathbf{r})}, \quad (1)$$

with a sum over all sites in a unit cell. We spherically average functions over the solid angle ( $d\Omega = d\theta d\phi$ ) within  $|\mathbf{r}| \leq R_{\text{CS}}$ , the maximal region required in a site-centered method. We then accurately integrate over the interstitial region of arbitrary VP (full shape) via isoparametric integration,<sup>26</sup> which is fast with error controllable to machine precision. We note that approximations to Eq. (1) reproduce various well-known simplified expressions used for decades, such as the muffin-tin and ASA cases, but these lead to poorer results generally.

The total energies can be evaluated using weighted VPs, denoted by KKR-CPA(VP), or weighted VPs approximated by unequal ASA spheres, denoted by KKR-CPA(ASA). For comparison, we also provide equal ASA sphere results, often used in other ASA-based codes. Definition (1) yields kinetic energies that approach those of LAPW.<sup>19</sup> For ordered and disordered (i.e., CPA and SQS) results, we find significantly improved predictions using optimal SPR basis within each VP, in combination with the  $v_0^{\text{VP}}$ , even if the remainder of the calculations is based on ASA, as exemplified for Al-Li. The CPA is applicable to an arbitrary  $x$  (solid solutions and partially ordered states<sup>2</sup>), and configurational averages can be improved, for example, by dynamical cluster approximation.<sup>30</sup>

### III. RESULTS

We report formation and mixing enthalpies ( $\Delta E_f$ ), impurity formation (or solution) energies ( $\Delta E_{\text{imp}}^x$ ), and lattice constant ( $a$ ) changes versus composition ( $x$ ). We address the critical charge representation in electronic-structure methods to make predictions from various theoretical techniques more consistent. For Al-Li, comparing to experimental data should be done with care, as the literature contains large scatter in

various values. It is also well known that there is a Li deficiency that extends 0.3 nm into the bulk from the surface in Al-Li alloys.<sup>31</sup> Hence, experiments affected by this deficient region will not provide reliable data versus  $x$ .

#### A. (Dis)ordered formation energies

Our results will clearly demonstrate that KKR-CPA(VP) correctly predicts the stability of ordered, disordered, and partially ordered phase all within the same fast code.<sup>25</sup> In Fig. 1 (bottom panel) we show the  $\Delta E_f$  versus  $x$  for ordered Al <sub>$m$</sub> Li <sub>$n$</sub>  [ $x = n/(n+m)$ ] and disordered Al<sub>1- $x$</sub> Li <sub>$x$</sub>  alloys. Selected values of the results are provided in Table I and compared with LAPW and available experimental data, as well as ASA results, such as from linear and exact<sup>33</sup> MTO (EMTO) methods.

Importantly, using an SPR optimal basis and Eq. (1), the KKR-CPA(VP) results for compounds are now in excellent agreement with LAPW results<sup>19</sup> and measured data.<sup>32</sup> For example, the measured  $\Delta E_f^{\text{B32}}$  is  $-252 \pm 10$  meV and our optimal-basis KKR(VP) result is  $-264$  meV ( $-276$  meV) at

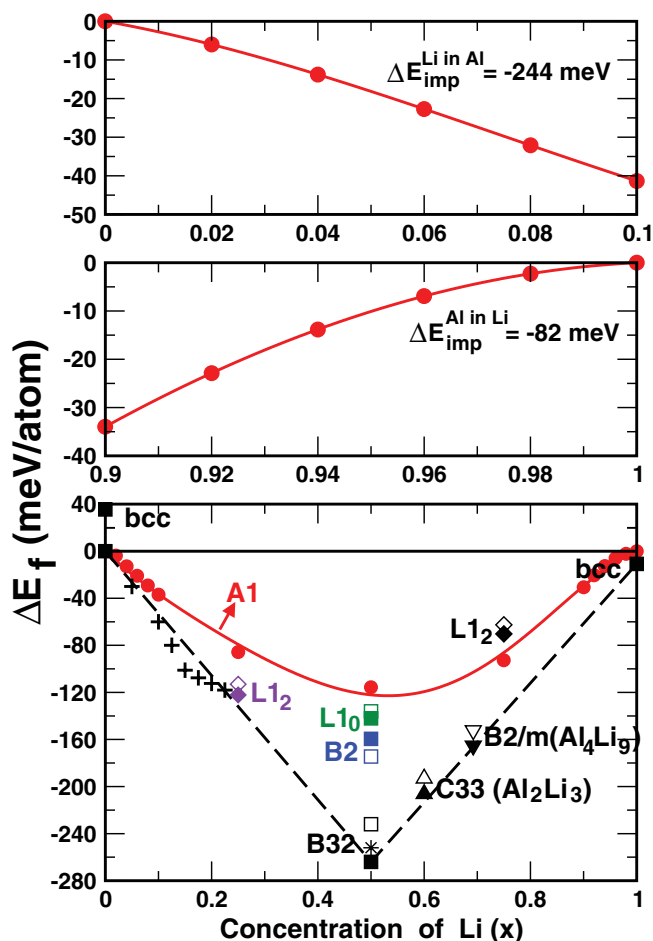


FIG. 1. (Color online) (Bottom)  $\Delta E_f$  (meV/atom) vs  $x$  of Al Al<sub>1- $x$</sub> Li <sub>$x$</sub> , and various fcc- and bcc-based compounds. KKR [LAPW (Ref. 19)] results are solid (open) symbols; B32 experiment (Ref. 32) (\*); A1 phase (solid curve); ground-state hull (dashed lines); and Al-rich (off-stoichiometric) L1<sub>2</sub> (pluses). Impurity formation energy  $\Delta E_{\text{imp}}$  (meV/atom) is from a limit of a fit to  $\Delta E_f$  (middle) Al in Li ( $0.9 < x < 1.0$ ) and (top) Li in Al ( $0 < x < 0.1$ ), values indicated in figure.

TABLE I.  $\Delta E_f$  (in meV/atom) for (dis)ordered alloys with equal and weighted-SPR-VP spheres relative to elements in same phase, using the variational  $v_0$  [Eq. (1)]. CPA and SQS results are from this work. CC denotes combined corrections. Other results are also given.

System	Method	Equal sphere		SPR sphere	
		$\Delta E_f^{\text{ord}}$	$\Delta E_f^{\text{dis}}$	$\Delta E_f^{\text{ord}}$	$\Delta E_f^{\text{dis}}$
A1-A2	KKR-ASA(VP)			-35.5	
Al	LAPW <sup>11</sup>			-62.6	
	EMTO <sup>33</sup>			-39.4	
	KKR-ASA			-19.0	
L1 <sub>2</sub> /A1	KKR-CPA(VP)	-78.3	-4.6	-122	-86
Al <sub>3</sub> Li	KKR-SQS-16(VP)		-33.5		-65
	LAPW <sup>11</sup>			-113	
	EMTO <sup>33</sup>			-111	
	ASW-ASA <sup>20</sup>			-109 <sup>a</sup>	
	KKR-CPA(ASA)	-47.7	-53.9	-133	-91
	KKR-SQS-16(ASA)		-55.1		-55
	LMTO-ASA-CC <sup>34</sup>	-75.6	n/a	-134 <sup>b</sup>	n/a
LMTO-CPA-ASA <sup>34</sup>	-57.4	+91.1	-283 <sup>c</sup>	-265 <sup>c</sup>	
L1 <sub>0</sub> /A1	KKR-CPA(VP)	-71.8	-54.2	-142	-116
AlLi	KKR-SQS-8(VP)		-55.7		-116
	LAPW <sup>11</sup>			-140	
	EMTO <sup>33</sup>			-157	
	KKR-CPA(ASA)	-58.3	-32.3	-160	-127
	KKR-SQS-8(ASA)		-47.2		-98
	LMTO-CPA-LDA <sup>23</sup>				-102
	B32/A2	KKR-CPA(VP)	-187.8	-36.3	-264 <sup>d</sup>
AlLi	KKR-CPA(VP) <sup>e</sup>			-276 <sup>e</sup>	
	KKR-SQS-8(VP)		-65.7		-121
	Expt <sup>32</sup>			-252	
	LAPW <sup>19</sup>			-233	
	EMTO <sup>33</sup>			-295	
	KKR-CPA(ASA)	-180	-39.4	-280	-143
	KKR-SQS-8(ASA)		-67.2		-153
B2 AlLi	KKR-CPA(VP)	-118.2		-160	
	LAPW <sup>11</sup>			-142	
	EMTO <sup>33</sup>			-190	
	KKR-CPA(ASA)	-109.2		-139	
	LMTO-ASA-CC <sup>12</sup>			-141	
L1 <sub>2</sub> /A1	KKR-CPA(VP)			-70	-93
AlLi <sub>3</sub>	KKR-SQS-16(VP)				-78
	KKR-SQS-16(VP) <sup>f</sup>				-97 <sup>f</sup>
	LAPW <sup>11</sup>			-68	
	EMTO <sup>33</sup>			-91	
A1-A2	KKR-ASA(VP)			+8.2	
Li	LAPW <sup>11,19</sup>			-6.8	
	EMTO <sup>33</sup>			-3.9	
	KKR-ASA			+4.1	

<sup>a</sup>Adjusted spheres via pseudopotential theory (see text).

<sup>b</sup>Charge-neutral, adjusted spheres with CC and  $L_{\text{max}} = 2$ .

<sup>c</sup>Charge-neutral, adjusted spheres with  $L_{\text{max}} = 2$ .

<sup>d</sup>Using experimental lattice parameters at 300 K.

<sup>e</sup>Using theory minimized lattice parameters at 0 K.

<sup>f</sup>Includes relaxation of SQS-16 from Ref. 4 (see text).

the experimental 300 K  $a = 6.369$  Å (0 K theory  $a = 6.276$  Å) lattice constant, while LAPW finds  $-232$  meV. (The 0 K experimental  $a$  will agree better with theory, as is typical.) For metastable L1<sub>0</sub> AlLi,  $\Delta E_f^{L1_0}$  is  $-142$  meV for KKR(VP)

and  $-140$  meV for LAPW; both  $a$  and  $c$  at 0 K are within 1.4% compared to experimental values at 300 K, but again experiment would be closer to theory if extrapolated to 0 K.  $\Delta E_f^{B2}$  for metastable B2 (CsCl) phase, predicted to exist at

high pressure,<sup>12</sup> is  $-160$  meV for KKR(VP) and  $-142$  meV for LAPW.

The KKR-CPA mixing enthalpy  $\Delta H_f^{A1}(x)$  for disordered fcc Al-Li is shown by the solid (red) curve in Fig. 1. Generally, in phase diagram assessments, the solid-solution enthalpy of a fixed phase is fitted to a polynomial in  $x$ , such as

$$\Delta H_f^{A1}(x) = \sum_{m,n} L_{mn} x^m (1-x)^n \quad \forall (m+n) \leq 4, \quad (2)$$

where  $L_{mn}$  are the polynomial coefficients. For Al-Li, the asymmetry in the  $\Delta H_f^{A1}(x)$  in Fig. 1 arises from the Madelung contributions to the total energy, which is proportional to  $(\Delta Q_i)^2$ , the effective charge on a site, which also has a corresponding asymmetrical form as a function of  $x$ . Therefore, site charge is an important quantity in Al-Li, and a proper description of charge density and the corresponding transfer effect is necessary, as is discussed below.

### 1. (Off)stoichiometric Al-rich L1<sub>2</sub>

The observed miscibility<sup>16</sup> of L1<sub>2</sub>-Al<sub>3</sub>Li with respect to Al-Al and B32-AlLi is reproduced. Indeed, the segregation line between pure Al and B32 sits at  $-132$  meV at 25% Li, whereas L1<sub>2</sub> is  $-122$  meV, that is, barely unstable but a very low-energy excitation; and, concomitantly, the stability of L1<sub>2</sub>-Al<sub>3</sub>Li relative to Al-Al<sub>0.75</sub>Li<sub>0.25</sub> yields the observed L1<sub>2</sub> precipitation within the  $\alpha(\text{Al}) + \beta$  two-phase field.<sup>16</sup> L1<sub>2</sub> remains metastable as free energies of the competing ordered phases change little because their order is near perfect, whereas that of the Al-rich disordered phase decreases rapidly due to the increasing solubility of Li and the increasing configurational entropy.

This argument can be supported by looking at the energetics for Al-rich, off-stoichiometric L1<sub>2</sub>, shown as plus symbol in the lower panel of Fig. 1, where the excess Al goes only to a Li corner-site and the three Al face sites remain fully occupied by Al. These data indicate that a partially disordered arrangement on the Al-rich side is more stable than the Al phase, and, by comparing to the ground-state hull, slightly more favorable than  $\alpha(\text{Al}) + \beta$  alone. Based only on 0 K enthalpy differences, we directly predict a higher stability of off-stoichiometric L1<sub>2</sub> between 8% and 20% Li with a peak at  $\sim 15\%$ , as observed<sup>17</sup> for the  $\delta'(\text{Al}_3\text{Li})$  precipitates, where it undergoes a transformation to  $\alpha(\text{Al}) + \delta(\text{AlLi})$  state at  $\sim 618$  K.<sup>17</sup> At the 15% peak, we estimated the maximum order-disorder temperature from  $\Delta E_f^{A1-\delta'(L1_2)}$  as 581 K. Also, at perfect stoichiometry  $\Delta E_f^{A1-L1_2}$  is 42 meV (or 488 K) and it compares well with the 522 K obtained via a much more involved CE fit using LAPW results.<sup>11</sup> These theory results should be compared to the measured eutectic temperature (869 K), showing that the liquid free energy is more favorable than the two-phase and homogeneous solid solution.

### 2. CPA vs SQS

For completeness, we compare the CPA to the SQS, within the same code and approximations. The SQS is an ordered cell meant to approximate the two-site atomic correlations of a random alloy to a small cutoff, but it does not include configurational averaging as in the CPA, except as offered by

the limited number of inequivalent sites within the ordered local environments. In Table I, we compared our SQS and CPA results at 25% and 75% (a 16-atom cell<sup>10</sup>) and at 50% (an average of two 8-atom configurations,<sup>9</sup> one state having large positive formation energy and the other negative, as is typical). They agree from 2% to 20% depending on composition  $x$ , but only if the SPR basis is used for both, as can be verified in Table I; both CPA and SQS are sensitive to basis representation but agree reasonably well within the optimal SPR basis, especially if larger SQS cells are used to improve the effective configurational average (see fcc 50% case, e.g., in Table I, where VP results show much improved agreement). Also, for the SQS-AlLi<sub>3</sub>, relaxation of this ordered cell (an approximate to the disordered phase) leads to a decrease<sup>4</sup> of energy by 19 meV, which improves the SQS agreement with the CPA (see Table I), where SQS formation energy becomes  $-97$  meV (i.e.,  $-19 - 78$  meV) compared to CPA's  $-93$  meV. The SQS-Al<sub>3</sub>Li relaxation is relatively small,  $\simeq 1$  meV.

### B. Impurity formation energies

We now address the solution enthalpy (or impurity formation energy), a more sensitive quantity to the approximations used, because they are related to the slope of the formation energy in the impurity limits. In the top and middle panels of Fig. 1, we show  $\Delta E_f$  vs  $x$  for Al phase in the two extreme limits ( $0 \leq x \leq 0.1$  and  $0.9 \leq x \leq 1.0$ ). The solution enthalpy must be determined from Eq. (2) using two restricted fits in the limits, that is, for B in A ( $0 \leq x \leq 0.1$ ) and vice versa ( $0.9 \leq x \leq 1.0$ ),

$$\begin{aligned} \Delta E_f^{x \rightarrow 0(1)} &= \sum_{m,n} L_{mn}^{x \rightarrow 0(1)} x^m (1-x)^n, \\ \Delta E_{\text{imp}}^{\text{B in A}} &= \left[ \frac{\partial}{\partial x} \Delta E_f^{x \rightarrow 0} \right]_{x=0}, \\ \Delta E_{\text{imp}}^{\text{A in B}} &= - \left[ \frac{\partial}{\partial x} \Delta E_f^{x \rightarrow 1} \right]_{x=1}, \end{aligned} \quad (3)$$

where  $L_{mn}^{x \rightarrow 0(1)}$  are the restricted fitting coefficients. The slopes at each end point are very different from one another and cannot be reliably extracted by a polynomial fit for all  $x$  from Eq. (2), as typically done.

Using Eq. (3) and our KKR-CPA(VP) results, our  $\Delta E_{\text{imp}}^{\text{Li in Al}}$  is  $-244$  meV/atom and  $\Delta E_{\text{imp}}^{\text{Al in Li}}$  is  $-82$  meV/atom. A thermodynamic fit to experimental data using CALPHAD yields<sup>35</sup>  $-222$  meV/atom for  $\Delta E_{\text{imp}}^{\text{Li in Al}}$  and  $-154$  meV/atom for  $\Delta E_{\text{imp}}^{\text{Al in Li}}$ . Our present results now agree much better with this one set of estimated experimental data, where notably only the Al-rich side has Al measured data. In the Li-rich end, by using the CPA results in the impurity limit, the relaxation effect of a single Al impurity around Li is not taken into account. A small increase in the magnitude of our calculated  $\Delta E_{\text{imp}}^{\text{Al in Li}}$ , will improve our results versus CALPHAD, as also suggested by the SQS results with larger relaxation at Li-rich end.

Midownik<sup>36</sup> has shown, however, that phase diagram fitting is not always able to predict structural energy differences accurately; hence, there is significant variation in the literature. For example, for Li in Al and Al in Li, other CALPHAD fits yield  $-131$  meV/atom and  $+972$  meV/atom,<sup>37</sup> respectively,

the later being unphysical; and, another CALPHAD fit yields  $-954$  meV/atom and  $-130$  meV/atom,<sup>38</sup> respectively, giving a phase diagram not in very good agreement with the experiment.<sup>35</sup>

Other theory results are in quantitative disagreement to experiment and the present results; for example, previous SQS results for  $\Delta E_{\text{imp}}^{\text{Li in Al}}$  find  $-309$  meV/atom, and cluster expansions yields  $-353$  meV/atom, while former equal-sphere CPA results give  $-358$  meV/atom.<sup>4</sup> All previous values were consistent, but none were obtained from proper impurity limit. Discrepancies between results of the various electronic-structure based methods (CPA, CE, SQS, etc.) have been explained using Al-Ag alloys as case study,<sup>3</sup> where charge issues were not significant, whereas for Al-Li the charge representation is crucial, as noted for “big-atom/small-atom” alloys.<sup>2,26</sup>

### C. Lattice constants

The minimized  $a$  vs  $x$  for Al  $\text{Al}_{1-x}\text{Li}_x$  (solid curve) is shown in Fig. 2, as well as that for bulk  $\text{Li}_2\text{Al}_3\text{Li}$  (square), with dilute limit slope added (dashed line) reproducing the well-known strong deviation to Vegard’s rule (dot-dashed line). Although the atomic volume of Li is 20% larger than that of Al, addition of Li to Al initially causes a contraction of  $a$  vs  $x$ , which we also find in quantitative agreement with experiment.<sup>16,40,42</sup> Various experimental  $a$ ’s reported<sup>16,40-42</sup> are indicated by symbols, including Al-rich Al and  $\delta'$ ( $\text{Al}_3\text{Li}$ ) precipitates. First, our calculated  $a$  for pure Al at 0 K is in agreement with experiment.<sup>39</sup> Our results do not include thermal expansion effects, which are in room-temperature measurements, explaining the  $-0.7\%$  difference in calculated results. Experimentally,<sup>16</sup>  $a$  for  $\delta'$ ( $\text{Al}_3\text{Li}$ ) at RT shrinks by 1% compared to pure Al (see Fig. 2), and we find a reduction of 1.25% at 0 K, in agreement with experiment (accounting for thermal expansion makes the agreement even closer). Finally, a very sensitive measure is the slope of the  $a$  vs  $x$  curve near Al, which is measured<sup>40,42,43</sup> to be  $-2.9$  to  $-6.9 \times 10^{-5}$  nm per

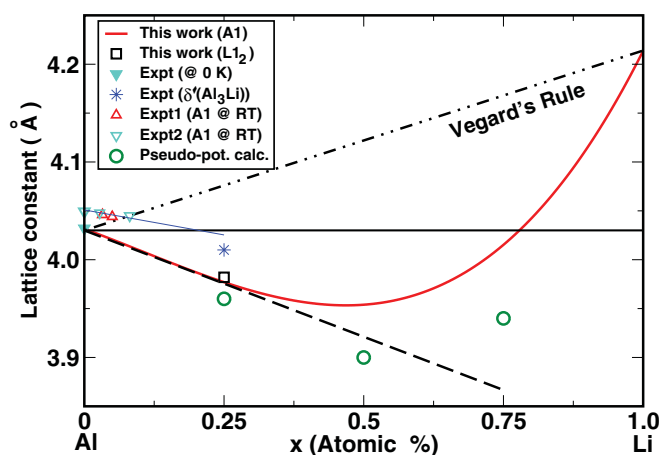


FIG. 2. (Color online) KKR-CPA(VP)  $a$  vs  $x$  for Al- $\text{Al}_{1-x}\text{Li}_x$  [solid (red) curve], compared to other data, including  $a_{\text{expt}}^{\text{Al}}$  at 0 K (Ref. 39)  $a_{\text{expt}}^{\text{Al}}$  from room temperature (RT) measurements [down (Ref. 40) and up (Refs. 41 and 42) triangles].  $a_{\text{expt}}$  for  $\delta'$ ( $\text{Al}_3\text{Li}$ ) precipitate at 523 K [\* (Ref. 16)]. Also shown are pseudopotential results via first-order perturbation theory (open circles).<sup>20</sup>

at.% Li and at 300 K. The FLAPW impurity doping results<sup>11</sup> give  $-5.1 \times 10^{-5}$  nm per at.% Li. Using the CPA at 0 K, we find it to be  $-11 \times 10^{-5}$  nm per at.% Li.

### D. ASA vs VP

For completeness, we provide the energetics from a wholly ASA implementation, including with  $v_0^{\text{ASA}}$  in Eq. (1) evaluated using ASA spherical (not VP) integrals, denote as KKR-CPA(ASA). Moreover, to better understand the sensitivity of the effective charge and Madelung energy, the calculations are done in two different ways: (1) standard equal atomic size (sphere or VP) for both Al and Li atoms (as done in many calculations) and (2) adjusting the sizes of each site by a weighted VP from the SPR found in a given environment.<sup>5</sup> From Table I, the SPR basis yields significantly improved energetics (especially compared to equal sphere ASA case) for both ordered and disordered phases, and eliminates the basis-set dependence for energy difference.<sup>5</sup> For instance, the SPR KKR-ASA result for ordered  $\text{Li}_2\text{Al}_3\text{Li}$   $\Delta E_f^{\text{Li}_2}$  is  $-133$  meV/atom and it is in dramatic contrast to the equal-sphere KKR-ASA result of  $-47.7$  meV/atom. Improving the SPR-ASA basis using  $v_0^{\text{VP}}$  and VP integrations [i.e., KKR-CPA(VP)] yields  $\Delta E_f^{\text{Li}_2} = -122$  meV/atom, in better agreement with  $-113$  meV/atom from LAPW.<sup>19</sup>

### E. Charge representations

The phase stability and the bonding characteristics of the Al-Li alloys can be understood by looking at distribution of valence charge around each atom. A characteristic of this compound is that Li-atom redistributes some of its valence electron in between the Al bonds and the resultant strengthened Al bonds stabilize the compounds. The charge density topology in the Li-rich compounds is more crucial in stabilizing a particular phase.

In Table II, the calculated local excess charges are provided within ASA and weighted VP for some ordered and disordered phases. The corresponding inscribed sphere (MT) and the ASA radii are given in Table III. From Table II, it is clear that there is a significant “charge transfer” from Li to Al for both ordered and disordered phases, as expected from electronegativity, where Al (1.61) is larger than Li (0.98). The excess (deficit) SPR-VP site charges from the KKR-CPA(VP), as expected, reflect a better charge neutrality than the SPR-ASA site charges more approximate KKR-CPA(ASA). The KKR-CPA(VP) thus provides an improved estimate of the chemical potential and energetics, as shown, as well as charge effect due to the more proper charge density representation. In a VP-based calculation, Madelung contribution to the total energy, as compared to an ASA, is minimized.

For the optimal SPR basis, the inscribed sphere reflects more appropriately the extent of the charge density on an atomic site, and hence a more reliable estimate of site charges; also the case for the unequal SPR-ASA results, but the energetics are sensitive to VP integrations. For example, in AlLi for the SPR-VP basis, the excess (deficit) charge on Al (Li) remains almost unchanged for A2 and B32 phases (with only  $0.005e^-$  exchanged to Li from Al), whereas for the

TABLE II. Excess charges for equal and weighted SPR of Li (first line) and Al (second line) atoms in (dis)ordered Al-Li.

System	Method	Equal		SPR	
		$\Delta Q^{\text{ord}}$	$\Delta Q^{\text{dis}}$	$\Delta Q^{\text{ord}}$	$\Delta Q^{\text{dis}}$
L1 <sub>2</sub> Al <sub>3</sub> Li	KKR-CPA(VP)	-0.450	-0.291	-0.126	-0.108
		+0.150	+0.097	+0.042	+0.036
	KKR-CPA(ASA)	-0.498	-0.303	-0.141	-0.132
		+0.166	+0.101	+0.047	+0.044
L1 <sub>0</sub> AlLi	KKR-CPA(VP)	-0.101	-0.069	-0.032	-0.026
		+0.101	+0.069	+0.032	+0.026
	KKR-CPA(ASA)	-0.130	-0.099	-0.082	-0.058
		+0.130	+0.099	+0.082	+0.058
B32 AlLi	KKR-CPA(VP)	-0.203	-0.187	-0.050	-0.045
		+0.203	+0.187	+0.050	+0.045
	KKR-CPA(ASA)	-0.236	-0.197	-0.098	-0.105
		+0.236	+0.197	+0.098	+0.105
B2 AlLi	KKR-CPA(VP)	-0.080		-0.025	
		+0.080		+0.025	
	KKR-CPA(ASA)	-0.100		-0.068	
		+0.100		+0.068	

SPR-ASA sphere the charge remains small but is double that of the VP result.

For the equal-sphere ASA results, however, there is an unphysical deficit charge on the smaller atom (Li) from the improperly described tails of the charge density of larger atom (Al), which have been arbitrarily cut off at the smaller radii (hence, the dependence upon charge representation of the basis set we discussed). The equal sphere results are unphysical, and the large charge exchange significantly impacts the total energy results (see discussion in Sec. IV), which is also responsible for the enormous variation in past DFT results.

#### IV. DISCUSSION

Unlike other arbitrary (or unphysical) choices of charge density representation and basis set, the present SPR-based basis (weighted VP or ASA spheres) provides a unique, physics-based optimal representation of the charge topology for each atom type in a given environment. This new basis reflects more properly the electronegativity (“charge transfer”), reduces the overlap error for ASA, and is valid for both ordered

TABLE III. Saddle-point based inscribed sphere MT and ASA radii (in Å) for Al and Li atoms in (dis)ordered Al-Li.

System	Atom	MT radius		ASA radius	
		$R_{\text{MT}}^{\text{ord}}$	$R_{\text{MT}}^{\text{dis}}$	$R_{\text{ASA}}^{\text{ord}}$	$R_{\text{ASA}}^{\text{dis}}$
L1 <sub>2</sub> Al <sub>3</sub> Li	Al	1.456	1.446	1.606	1.600
	Li	1.288	1.312	1.458	1.481
L1 <sub>0</sub> AlLi	Al	1.484	1.467	1.639	1.627
	Li	1.326	1.337	1.498	1.513
B32 AlLi	Al	1.418	1.417	1.602	1.613
	Li	1.299	1.295	1.499	1.509
B2 AlLi	Al	1.457	1.645		
	Li	1.253	1.472		

and disordered alloys, that is, CPA and SQS approximations. For the sensitive case of Al-Li this has been demonstrated, which permits direct calculation of fully ordered, partially ordered, and disordered alloys, as recently shown for the quantum criticality in the doped, intermetallic NbFe<sub>2</sub>,<sup>24</sup> and magnetic-storage alloys.<sup>2</sup>

Previously, Masuda-Jindo and Terakura<sup>20</sup> applied pseudo-potential-based, first-order perturbation theory<sup>44</sup> to reveal a contraction in  $a$  versus  $x$  for Al-rich solid solutions, similar to experiment, which deviates from a simple Vegard’s rule due to effects from bulk moduli and atomic volumes. They derived a relation for a mean ASA radii versus  $x$  for the alloy, which was then used to perform a KKR-ASW study<sup>20</sup> of solid-solution hardening and softening using only ordered structures (Al<sub>7</sub>Li and Al<sub>3</sub>Li). For L1<sub>2</sub>-Al<sub>3</sub>Li they found a decrease of  $a$  by 1.5% compared to pure Al. In light of our present results, their adjustments to the ASA radii better reflect the electron density and “charge transfer,” in agreement with our SPR-based VP and ASA.

Korzhevyyi *et al.*<sup>23</sup> performed LMTO-CPA-ASA calculations for the random alloy using charge corrections (similar to the scr-CPA) with an adjustable parameter and *a posteriori* correction for apparent charge transfer given by their choice of ASA spheres. Only then did they find that the  $a$  versus  $x$  and mixing enthalpy started to agree qualitatively with experiment. No such *a posteriori* choices and corrections are needed for our optimal basis, uniquely chosen before any calculation.<sup>5</sup>

Finally, in an attempt to correct the apparent “errors” of the CPA, Singh and Gonis<sup>34</sup> proposed “charge-neutral” spheres, an arbitrary, unphysical, and, as recently discussed,<sup>5</sup> unnecessary assignment. Their formation energy changed from positive to negative when the spheres’ radii were adjusted to give charge neutrality, with the latter giving a clearly incorrect formation enthalpy of  $-283$  ( $-265$ ) meV for the ordered (disordered) Al<sub>3</sub>Li, as shown in Table I. For the ordered alloys, however, they were able to add *combined corrections* to the LMTO-ASA, which reduces ASA overlap errors due

to the approximately 50% increase in the Al ASA radii. With combined corrections the  $L1_2$  formation enthalpy improves to  $-134$  meV; yet, they could not correct the CPA in a similar fashion. Such an approach, however, does not represent the CPA charge density correctly.<sup>5</sup> Simply put, for Al-Li, such a dramatic change in ASA radii to force charge neutrality arises solely because of the large difference in calculated bulk moduli (Al 0.72 Mbar vs Li 0.12 Mbar) and volumes (Al 3.981 Å and Li 4.255 Å). Hence, only for ASA, the Al sphere will enlarge at the expense of Li because the Li sphere is easily compressed (the ratio of Al to Li bulk moduli is 6), so the size of the Li sphere is expected to decrease much more than should be physically expected from the total density (see original motivations discussed in Refs. 20 and 5). So, when the moduli are substantially different, this adjustment does not describe the proper density, and adjusting spheres to minimize energy, say, is unwarranted.

Generally, however, using the SPR from the electronic density as the inscribed sphere of the VP (and using radical plane construction weighting to define full VP) offers a unique, physical, and optimized representation, working for all ordered and disordered configurational averaging approximations, including the CPA.

## V. SUMMARY

For the commercially important Al-Li system, using a unique, physical and optimized representation of a site-centered charge density and potential in any local configuration using the KKR-CPA, we accurately predicted the relative stability of all ordered, off-stoichiometric partially ordered and disordered phases, including thermal antisites.<sup>6</sup> We also resolved long-standing discrepancies throughout the literature for the sensitivity of Al-Li energy estimates for disorder alloys (CPA, SQS, and CE), permitting accurate prediction of formation enthalpies, solution enthalpies, and structural properties for general alloy configurations, all within a single code as desired for a reliable study of phase stability in complex alloys.

## ACKNOWLEDGMENTS

This work was supported by the US Department of Energy, Office of Basic Energy Science, Division of Materials Science and Engineering (DE-FG02-03ER46026, algorithm development) and Ames Laboratory (DE-AC02-07CH11358, materials discovery applications). Ames Laboratory is operated for the US Department of Energy by Iowa State University.

\*aftab@ameslab.gov

†ddj@ameslab.gov

<sup>1</sup>P. E. A. Turchi, M. Sluiter, F. J. Pinski, D. D. Johnson, D. M. Nicholson, G. M. Stocks, and J. B. Staunton, *Phys. Rev. Lett.* **67**, 1779 (1991).

<sup>2</sup>Aftab Alam, Brent Krazcek, and D. D. Johnson, *Phys. Rev. B* **82**, 024435 (2010).

<sup>3</sup>D. D. Johnson and Mark Asta, *Comput. Mater. Sci.* **8**, 54 (1997).

<sup>4</sup>M. H. F. Sluiter and Y. Kawazoe, *Europhys. Lett.* **57**, 526 (2002).

<sup>5</sup>Aftab Alam and D. D. Johnson, *Phys. Rev. B* **80**, 125123 (2009).

<sup>6</sup>D. D. Johnson, A. V. Smirnov, J. B. Staunton, F. J. Pinski, and W. A. Shelton, *Phys. Rev. B* **62**, R11917 (2000).

<sup>7</sup>D. D. Johnson, D. M. Nicholson, F. J. Pinski, B. L. Gyorffy, and G. M. Stocks, *Phys. Rev. Lett.* **56**, 2088 (1986); *Phys. Rev. B* **41**, 9701 (1990).

<sup>8</sup>D. D. Johnson and F. J. Pinski, *Phys. Rev. B* **48**, 11553 (1993).

<sup>9</sup>Alex Zunger, S.-H. Wei, L. G. Ferreira, and James E. Bernard, *Phys. Rev. Lett.* **65**, 353 (1990); Z. W. Lu, S.-H. Wei, and Alex Zunger, *Phys. Rev. B* **44**, 10470 (1991).

<sup>10</sup>C. Wolverton, *Acta Mater.* **49**, 3129 (2001).

<sup>11</sup>M. Sluiter, D. de Fontaine, X. Q. Guo, R. Podlucky, and A. J. Freeman, *Phys. Rev. B* **42**, 10460 (1990).

<sup>12</sup>M. H. F. Sluiter, Y. Watanabe, D. de Fontaine, and Y. Kawazoe, *Phys. Rev. B* **53**, 6137 (1996).

<sup>13</sup>Nikolai A. Zarkevich and D. D. Johnson, *Phys. Rev. Lett.* **92**, 255702 (2004).

<sup>14</sup>A. J. McAlister, *Al-Li (Aluminum-Lithium), Binary Alloy Phase Diagrams*, II Ed., edited by T. B. Massalski (ASM International, Ohio, USA, 1990), Vol. 1, pp. 167–168.

<sup>15</sup>R. Poduri and L.-Q. Chen, *Acta Mater.* **45**, 245 (1996); B. Noble and S. E. Bray, *ibid.* **46**, 6163 (1998); J. P. Simmons, Ph.D. thesis, Carnegie Mellon University, 1992.

<sup>16</sup>E. J. Lavernia and N. J. Grant, *J. Mater. Sci.* **22**, 1521 (1987).

<sup>17</sup>S. Ceresara, G. Cocco, G. Fagherazzi, and L. Schiffini, *Philos. Mag.* **35**, 373 (1977).

<sup>18</sup>B. Noble, S. J. Harris, and K. Dinsdale, *J. Mater. Sci.* **17**, 461 (1982).

<sup>19</sup>X. Q. Guo, R. Podlucky, and A. J. Freeman, *Phys. Rev. B* **40**, 2793 (1989); X. Q. Guo, R. Podlucky, J. H. Xu, and A. J. Freeman, *ibid.* **41**, 12432 (1990); X. Q. Guo, R. Podlucky, and A. J. Freeman, *ibid.* **42**, 10912 (1990); M. J. Mehl, *ibid.* **47**, 2493 (1993).

<sup>20</sup>Kin-ichi Masuda-Jindo and K. Terakura, *Phys. Rev. B* **39**, 7509 (1989).

<sup>21</sup>J. Laverock, S. B. Dugdale, M. A. Alam, M. V. Roussanova, J. R. Wensley, J. Kwiatkowska, and N. Shiotani, *Phys. Rev. Lett.* **105**, 236401 (2010).

<sup>22</sup>V. G. Vaks and N. E. Zein, *J. Phys.: Condens. Matter* **2**, 5919 (1990).

<sup>23</sup>P. A. Korzhavyi, A. V. Ruban, S. I. Simak, and Yu. Kh. Vekilov, *Phys. Rev. B* **49**, 14229 (1994).

<sup>24</sup>Aftab Alam and D. D. Johnson, *Phys. Rev. Lett.* **107**, 206401 (2011).

<sup>25</sup>D. D. Johnson, A. Alam, and A. V. Smirnov, *MECCA: Multiple-scattering Electronic-structure Calculations for Complex Alloys (KKR-CPA Program, ver. 1.9)* (University of Illinois, Urbana, IL, 2008).

<sup>26</sup>Aftab Alam, S. N. Khan, Brian G. Wilson, and D. D. Johnson, *Phys. Rev. B* **84**, 045105 (2011).

<sup>27</sup>H. J. Monkhorst and J. D. Pack, *Phys. Rev. B* **13**, 5188 (1976).

<sup>28</sup>U. Von Barth and L. Hedin, *J. Phys. C* **5**, 1629 (1972).

<sup>29</sup>V. L. Moruzzi, J. F. Janak, and A. R. Williams, *Calculated Electronic Properties of Materials* (Pergamon, New York, 1978).

<sup>30</sup>D. A. Biava, Subhradip Ghosh, D. D. Johnson, W. A. Shelton, and A. V. Smirnov, *Phys. Rev. B* **72**, 113105 (2005).

<sup>31</sup>H. Ueda, A. Matsul, M. Furukawa, Y. Mlura, and M. Nemoto, *J. Jpn. Inst. Met.* **49**, 562 (1985).

- <sup>32</sup>I. Barin, O. Knacke, and O. Kubaschewski, *Thermochemical Properties of Inorganic Substances* (Springer-Verlag, Berlin, 1977).
- <sup>33</sup>L. Vitos, *Comput. Mater. Sci.* **18**, 24 (2000).
- <sup>34</sup>P. P. Singh and A. Gonis, *Phys. Rev. B* **49**, 1642 (1994).
- <sup>35</sup>A. J. McAlister, *Bull. Alloy Phase Diagrams* **3**, 177 (1982).
- <sup>36</sup>A. P. Midownik, in *Computer Modeling of Phase Diagrams*, edited by L. H. Bennet (AIME, Warrendale, PA, 1986), p. 253.
- <sup>37</sup>S. Chen, C. Jan, J. Lin, and Y. A. Chang, *Metall. Trans. A* **20**, 2247 (1989).
- <sup>38</sup>M. L. Saboungi and C. C. Hsu, *CALPHAD: Comput. Coupling Phase Diagrams Thermochem.* **1**, 237 (1977).
- <sup>39</sup>G. N. Kamm and G. A. Alers, *J. Appl. Phys.* **35**, 327 (1964).
- <sup>40</sup>H. J. Axon and W. Hume-Rothery, *Proc. R. Soc. London A* **193**, 1 (1948).
- <sup>41</sup>Ann S. Copper, *Acta Crystallogr.* **15**, 578 (1962).
- <sup>42</sup>S. H. Kellington, D. Loveridge, and J. M. Titman, *J. Phys. D: Appl. Phys.* **2**, 1162 (1969).
- <sup>43</sup>E. D. Levine and E. J. Rapperport, *Trans. Metall. Soc. AIME* **227**, 1204 (1963).
- <sup>44</sup>J. Hafner, *From Hamiltonians to Phase Diagrams* (Springer-Verlag, Berlin, 1987).